Pulsed Adsorbent Transport in a Countercurrent Adsorptive Reactor

L. A. M. van der Wielen, C. A. P. M. van Nunen, and K. Ch. A. M. Luyben
Kluyver Laboratory for Biotechnology, Delft University of Technology, Julianalaan 67 2628 BL Delft, The Netherlands

Selective countercurrent transport of dense adsorbent particles through pulsed multistage, liquid fluidized beds of light catalyst particles is attractive as the basis for new countercurrent adsorptive reactors. Its applications are expected to demand operation at high solids flows, and thus at high pulsation frequencies and volumes. The effect of high pulsation frequencies and volumes on the flows of liquid and solids is studied by model and experiment. The key parameter determining contactor behavior is the product of pulsation frequency and volume: the pulsed back flow. Its theoretical maximum (flooding condition) equals the liquid flow rate. High pulsation frequencies and volumes greatly affect the degree of liquid and solids mixing. The degree of liquid mixing increases exponentially with increasing pulsed back flow from plug-flow behavior (Pe = 10 – 100/stage) to complete mixing near the flooding condition. The solids mixing at low-to-moderate solids transport could be described with complete mixing at this stage. At higher solids transport, the extent of mixing slightly decreases toward two tanks-in-series per stage. The relations established allow for a preliminary design of a pulsed multistage fluidized-bed reactor at any low and high solids transport rate, as well as for the estimation of corresponding operating conditions.

Introduction

Multistage fluidized-bed contactors

After many more-or-less successful designs for continuous countercurrent adsorption and ion-exchange equipment, Cloete and Streat (1962, 1963) were the first to patent a relatively compact, generally applicable and stable system in the form of a multistage fluidized-bed contactor. The multistage fluidized-bed contactor is essentially a plug-flow contactor that is compartmentalized by perforated plates. The holes in the plates are larger than the fluidized particles. By the periodic decrease or increase of the superficial liquid velocity, part of the bed material is transported through the holes in the plate to a lower or higher compartment, respectively. Thus semicontinuous countercurrent or cocurrent transport can be achieved. The series of events is shown in Figure 1.

When properly designed, much of the operational stability of the MFB-contactor can be attributed to the reversed liquid flow, which inevitably drags the solids countercurrent to the time-averaged liquid flow. Furthermore, the absence of mechanical parts, the presence of the fluidized bed, and the periodic flow reversal minimizes the possibility of clogging of the bed and of particle breakage. The system has been investigated for various applications in the field of ion exchange (Bennett et al., 1984; Dodds et al., 1973; Van der Meer, 1984),

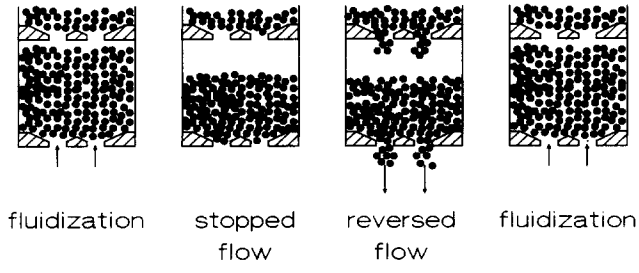

Figure 1. Pulsation cycle in one compartment and corresponding countercurrent solids transport, in a pulsed, multistage fluidized-bed contactor of the Cloete–Streat (1962) type.

Correspondence concerning this article should be addressed to L. A. M. van der Wielen.

Table 1 Characteristics of Reported Laboratory-Scale Multistage Fluidized-Bed Contactors of the Cloete–Streat Type

Author (System)	f_p Hz	ϵ_{2p}	V_p $\times 10^{-6}$ m^3	D cm	L m
Dodds et al. (1973) (Ion exchange)	0.017–0.033	—	—	7.6	0.51
Van der Meer (1984) (Ion exchange)	0.033	0.55	70–495	3	1
				12	3
Van der Wiel and Wesselingh (1989) (Sorption)	0.02–0.07	—	—	3	1
				12	3
				50	2
Vos et al. (1990) (Reaction)	< 0.01	0.66–0.73	15–120	3.54	1.8
Van der Wielen et al. (1995) (Reaction + separation)	0.02–0.5	0.87	5–101	3.54	1.8
				4.03	0.75

adsorption (Van der Wiel and Wesselingh, 1989), as a reactor for deactivating biocatalysts (DSM/Stamicarbon, 1980; Vos et al., 1990), and in a modified form, as an integrated adsorptive reactor (Van der Wielen et al., 1990, 1995). An overview of the reported studies is given in Table 1. Table 1 also incorporates reported values of key parameters, such as the range of pulsation frequencies f_p, the pulsation volume V_p, and its solids fraction ϵ_{2p}, column diameter D, and length L.

Particle segregation and a pulsed-flow reactor

In previous work (Van der Wielen et al., 1990, 1995), we have described a multistage fluidized-bed reactor that is capable of selective countercurrent transport of a "heavy" solid phase with retention of the "lighter" phase in the reactor. The terms heavy and light could be replaced by large and small particles. Fluidization of binary mixtures of particles with sufficiently different densities and/or sizes leads to segregation, resulting in a lower zone of the dense particles and in an upper zone of the lighter type. In a multistage setup as shown in Figure 2, this segregation resulted in an arrangement of alternating layers of dense and light particles.

The selection of adsorbent particles for the dense phase and an immobilized (enzyme) catalyst for the light phase results in a bottom adsorption zone and a top reaction zone in each compartment. By downward pulsation, part of the adsorbent material is transported from the bottom zone to a lower compartment, and the mixture of the remaining catalyst and adsorbent segregates again. Periodic pulsation results in semicontinuous countercurrent and selective transport of the adsorbent phase. This mechanism of the pulsed transport is shown in Figure 2. We will refer to this system as the pulsed-flow fluidized-bed reactor. A sufficiently selective adsorbent will ideally result in a product-loaded adsorbent flow from the bottom of the reactor. For example, in case of a hydrolysis reaction with two products, the application of a sufficiently selective adsorbent for one of the products might give an adsorbent flow from the bottom of the reactor containing one product and a liquid flow from the top containing the other (Van der Wielen et al., 1990, 1995, 1996b).

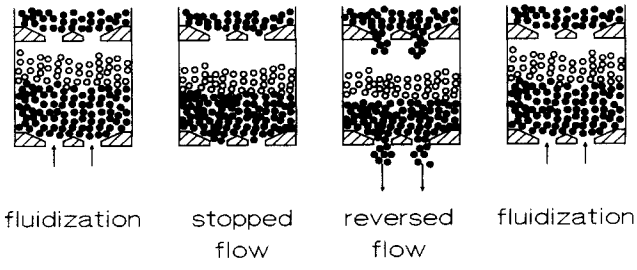

Figure 2. Series of events during selective countercurrent adsorbent transport in a pulsed, binary multistage fluidized-bed reactor, one compartment.

● Adsorbent particles; ○ biocatalyst particles.

Scope of this work

The existing literature on compact multistage fluidized contactors concerns systems that are either dilute in the component to be recovered or that contain a catalyst that deactivates relatively slowly. In both cases, the countercurrent solids transport is small when compared to the liquid flow. A typical ratio of the volumetric solids and liquid flow is 0.001–0.01. For an integrated adsorptive reactor, a high reactant concentration is preferred. This necessitates a large adsorbent flow to continuously and completely remove the product. Depending on actual reactant concentrations and maximum adsorption (ion-exchange) capacity of the dense solids, this results in a high adsorbent flow, most likely close to the flooding condition. In this case, the flooding condition is defined as the maximum solids feed rate to the contactor at given operating conditions. The flooding condition is determined by the maximum frequency and volume of the periodic flow reversals (pulsations). To our knowledge, the flooding condition of pulsed multistage fluidized beds has never been investigated. This is one of the aims of this article.

Furthermore, it is expected that operating close to the flooding condition leads to liquid and solids mixing behavior that deviates substantially from that previously reported. In the existing literature, the extent of plug flow of the liquid flow is high and the solid phase is completely mixed due to the long residence time of the solids relative to that of the liquid. In this work, the effect of pulsation frequency and volume on the extent of liquid and solids mixing is investigated as well.

Theory

Segregation in multicomponent fluidized beds

The underlying mechanism of the selective countercurrent transport of the dense or large particles in pulsed flow is the segregation of the dense/large and light/small fluidized particles. The final result will be separate layers. For systems with distinct differences in either size or density, the phase separation is predictable without a hydrodynamic model. However, the situation becomes less obvious when the sizes and densities of the particles become more and more similar, or for small, dense particles in combination with larger, light species. In the latter situation, the segregation and the corresponding location of the particles depend on the liquid velocity. Layer inversion and complete mixing of the particles have been observed and are well documented by, among others, Moritomi et al. (1982, 1986), Van Duijn and Rietema (1982),

Gibilaro et al. (1986), and Jean and Fan (1986). To predict whether or not stable segregation will occur for a given binary particle system, we start with a force balance for each component i in the binary particle system as given by Van der Wielen et al. (1996a):

$$F_{\text{gravity}} = F_{\text{buoyancy}} + F_{di}. \tag{1}$$

The overall suspension drag for the component, F_{di}, resulting from particle–liquid and particle–particle interactions, is described analogously to Foscolo and Gibilaro (1984):

$$F_{di} = \frac{\pi_{di}^3}{6}(\rho_i - \rho_L)g\left(\frac{\epsilon\nu_{Li}}{\nu_{Li\infty}}\right)^{4.8/n_i}\epsilon_L^{-3.8}, \tag{2}$$

with ν_{Li} being the (linear) slip velocity of component i: $(u_L - u_i)$. We assume equal particle–particle interaction between different particle species, and thus assume a completely hydrodynamic origin of the drag force. This results in

$$\rho_i - \bar{\rho} = (\rho_i - \rho_L)\left(\frac{\epsilon_L(u_L - u_i)}{\nu_{Li}^{\infty}}\right)^{4.8/n_i}\epsilon_L^{-3.8}. \tag{3}$$

The bulk density is determined by all phases present (Van Duijn and Rietema, 1982):

$$\bar{\rho} = \epsilon_L\rho_L + \epsilon_l\rho_l + \epsilon_2\rho_2, \tag{4}$$

and the sum of fractions equals unity:

$$1 = \epsilon_L + \epsilon_1 + \epsilon_2. \tag{5}$$

This set of equations relates particle velocities and holdups. Complete mixing of particles occurs when the actual slip velocities of the different particle species with the liquid are equal, hence when $\nu_{L1} = \nu_{L2}$. However, when different slip velocities result, the wanted phase separation will occur. By subtracting the slip velocities of the two species, we obtain the following criterion function F that indicates segregation:

$$F = \nu_{Ll,\infty}\left(\frac{\rho_1 - \bar{\rho}}{\rho_1 - \rho_L}\epsilon_L^{3.8}\right)^{n_1/4.8} - \nu_{L2\infty}\left(\frac{\rho_2 - \bar{\rho}}{\rho_2 - \rho_L}\epsilon_L^{3.8}\right)^{n_2/4.8}. \tag{6}$$

Substituting Eqs. 4 and 5 in Eq. 6, while eliminating ϵ_L, F is calculated for given particle properties as a function of the volume fractions of the two species. Negative values for F indicate sedimentation of species 2 (or floatation of species 1), whereas positive values of F indicate sedimentation of species 1 (or floatation of species 2). When F equals zero, the particles mix at that particular composition, resulting in an implicit relation between ϵ_1 and ϵ_2 at complete mixing. This nonlinear implicit relation can be solved numerically to relate the volume fractions of species 1 and 2 at complete mixing. However, Eq. 6 also may have no physically meaningful solution, indicating that the particle species do not mix in any combination. Hence, Eq. 6 can be used to select particle combinations as well as the desired operating conditions that favor segregation.

Countercurrent solids and liquid transport by pulsed flow

Solids Transport. The countercurrent flow of the dense adsorbent phase ϕ_2 is proportional to the frequency of pulsations f_p, the magnitude of the back-pulsed volume V_p, and its solids fraction ϵ_2:

$$\phi_2 = f_pV_p\epsilon_{2p}. \tag{7}$$

The frequency of the pulsations is limited by the slowest of two phenomena: relaxation of the bed and the segregation of the particles after the pulse.

The relaxation depends on the decay of the transient-wave phenomena corresponding to the settling, partial transport, and refluidization of the fluidized bed. A conservative criterion has been developed in previous work (Van der Wielen et al., 1997a), based on the propagation velocity of continuity waves in fluidized beds. The interested reader is referred for further details to that work. The overall relaxation time t_R can be estimated adequately from

$$t_R = t_C + \frac{\epsilon_L^{(2)}H^{(2)}}{nu_{Lo}^{(2)}(1 - \epsilon_L^{(2)})}. \tag{8}$$

Here, H is the bed height, u_{Lo} is the superficial liquid velocity, n the usual Richardson and Zaki exponent, and t_C is the cycle time of the actual flow reversal until the refluidization. Exponent (2) refers to the steady-state conditions after the pulse, and the second term at the righthand side of the equation considers the motion of the refluidization wave through the bed.

The time required for segregation can be computed from the segregation velocities and layer heights, using the force balance model presented by Van der Wielen et al. (1996a). For typical applications with resinous adsorbents in water, the segregation velocities are approximately 1–5 cm/s (Van der Wielen et al., 1996a, 1997b).

The fraction of the bed volume that can be transported during one pulsation is limited to about a third of the bed volume, for reasons of stability. The worst predictable parameter is the volume fraction of the solids in the pulsation volume. Values of 30–45% of solids have been mentioned by previous authors (Table 1, Van der Meer, 1984; Vos et al., 1990). As will be shown in the following sections, experimental determination of the solids fraction of the pulsation volume is still the most reliable option, but 30% can be used as a conservative estimate.

Liquid Transport. The magnitude of the time-averaged liquid flow is of course seriously reduced by the repeated flow reversals. During the actual flow reversal, the feed to the fluidized-bed column is stopped. Hence, for large pulsation frequencies and volumes, the solids transport increases and the time-averaged liquid flow declines. We assume that the total time during which the flow is stopped is proportional to pulsation volume and frequency. In practice, the transient liquid flow changes gradually and not abruptly. Therefore, the "stopped flow" time per pulsation cycle is also difficult to

estimate, but is approximated by the lower value of the relaxation time or segregation time. Hence, the liquid transport is described as follows:

$$\phi_L = \phi_{L0} - Cf_pV_p, \tag{9}$$

where C is an empirical constant, which reflects the actual reduction of the liquid flow by the complete back-pulsed flow. This constant is expected to be smaller than unity, and typically on the order of the volume fraction of the liquid in the pulsation volume. The liquid residence time is then given by

$$\tau_L = \frac{\tau_{L0}}{1 - C\dfrac{f_pV_p}{\phi_{L0}}} \quad \text{and} \quad \tau_{L0} = \frac{V}{\phi_{L0}}. \tag{10}$$

The performance of the pulsed-flow system when applied as an integrated reactor, is determined by the ratio of flow rates of adsorbent and liquid. The minimum ratio depends on adsorbent capacity and reactant concentration and can be estimated from a modified separation factor as shown in detail elsewhere (Van der Wielen et al., 1995, 1996b).

Liquid and solids mixing

In addition to axial dispersion in a steady-state or multistage fluidized-bed systems, enhanced liquid mixing is expected at high pulsation frequencies and pulsation volumes. A mechanistic description of the liquid-phase behavior during a pulsation can be obtained from a first-principles fluid dynamics model as presented in earlier work (Van der Wielen et al., 1997a). However, it is expected that the axial dispersion model describes the magnitude of the dispersion effect in sufficient detail. We therefore have used the axial dispersion model to analyze the residence time distribution of the liquid phase. The axial dispersion model reads in dimensionless form:

$$\frac{\partial c}{\partial \theta} = \frac{1}{Pe}\frac{\partial^2 c}{\partial z^2} - \frac{\partial c}{\partial z},$$

with $\theta = t/\tau_L$, $z = x/L$ and $Pe = (u_{Lo}\ L)/(\epsilon_L\ E)$. In the experimental procedure, tracer pulse-responses are monitored simultaneously at various locations in the system, so open-open boundary conditions are used. As is shown in a later section, the pulse responses are measured at various locations in the systems, typically at each stage. Then the tracer signal at a previous stage is used as the input for the succeeding stage, and this signal will have an arbitrary shape and will most certainly not be an ideal Dirac pulse. Therefore, the procedure outlined by Fahim and Wakao (1982), among others, has been used. In this method, the measured (and imperfect) signal is used as the initial condition for the axial dispersion model. The output signal $O(\theta)$ is then the convolution product of the input signal $I(\theta)$ and the transfer function of the bed, H. The latter is supplied by the axial dispersion model. The time-domain convolution is elaborate, but the convolution in the Fourier domain reduces to the mathematical product:

$$O(i\omega) = I(i\omega) \cdot H(i\omega). \tag{12}$$

The Fourier domain input signal $I(i\omega)$ is calculated from the experimental time-domain signal by standard mathematical procedures, in this case the fast Fourier transform. The Fourier-domain transfer function $H(i\omega)$ is obtained by Fourier transformation of the axial dispersion model, and subsequent decomposition of the solution into its real and imaginary parts. The Fourier-domain transfer function reads:

$$Re(H) = \exp(B)\cos[A\sin(C)];\ Im(H) = -\exp(B)\sin[A\sin(C)],$$

with

$$A = \frac{Pe}{2}|Z|^{0.5},\ B = \frac{Pe}{2} - A\cos(C) \quad \text{and} \quad C = \frac{\phi}{2} \tag{13}$$

$$|Z| = \left(1 + \left(\frac{4\omega\tau_L}{Pe}\right)^2\right)^{0.5} \quad \text{and} \quad \phi = \arctan\left(\frac{4\omega\tau_L}{Pe}\right).$$

By using the inverse of the fast Fourier transform algorithm, the Fourier-domain convolution product is transformed back to the time domain and is fitted to the experimental signal. This complete algorithm—signal transformation, convolution, and inverse transformation—was incorporated in an iterative Nelder-Mead, least-squares parameter fitting procedure to estimate Pe and τ_L.

The solids mixing is determined by step-response experiments. As shown in a later section, a compartment is filled with colored particles, which are washed out of the compartment by continuously feeding noncolored particles. Because the solids mixing is expected to be nearly complete at this stage, the solids mixing is modeled with one or two mixers in series.

Experimental Studies

Fluidized-bed system

The basic experimental setup has been described elsewhere (Van der Wielen et al., 1990) and is shown in Figure 3. The setup consists of a 0.75-m Perspex contactor with an internal diameter of 40.3 mm. The contactor is constructed of two sections to facilitate the adjustment of the perforated plates. The perforated plates are mounted at adjustable locations on a central axis, typically at 15 cm intervals. The system is equipped with a pulseless rotary-gear pump, a magneto-inductive flow meter, and a pulsation system as described by Vos et al. (1990). For this work, two pulsation tubes were used with a volume of 16×10^{-6} m^3 and 125×10^{-6} m^3, respectively. Both pulsation tubes contained a polypropylene float that was used to activate two optical sensors. These sensors monitored the pulsation cycle. The frequency of the pulsation was controlled by an electronic unit that also controlled the net flow of the rotary pump by opening or closing a valve in a recycle loop over the pump. The adsorbent supply at the top compartment was controlled using a differential optical solids level indicator consisting of two phototransistors taking advantage of the difference in color of the light (dark) and dense (white) solids phases.

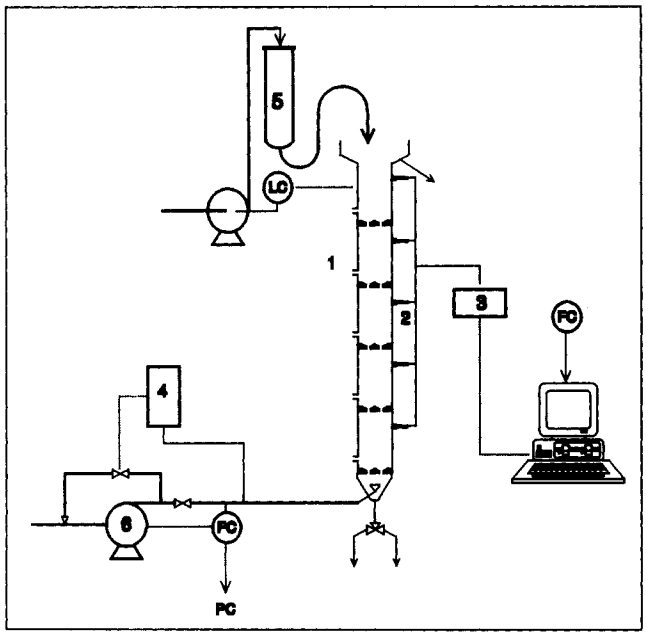

Figure 3. Laboratory-scale fluidized-bed system used for pulsed (shown) and trickle-flow experiments.

Perspex column (1); RTD measurement system (2,3); pulsation unit (4); dense phase supply (5); and gearless, rotary pump (6).

The distance between two subsequent perforated plates was 0.15 m, resulting in a compartment (stage) length of approximately 0.14 m. Each of these stages has two sample ports, located at 5 and 10 cm above the plate. These sample ports were used to withdraw samples from the reactor or to install sensors. To determine the residence-time distribution of the liquid, the column was equipped with a fiber-optic fluorimeter system as described by Groen (1994) and a number of conductivity electrodes of the type described by Khang and Fitzgerald (1975). For either system, pulse-response measurements were performed with sodium-fluorescine as a fluorescent salt. The injection of the salt pulse, the data-acquisition, and the timing of the liquid pulsation unit were controlled by a Hewlett-Packard Vectra ES/12 personal computer.

Particles

Immobilized glucose isomerase (Maxazyme GI Immob, Gist-brocades nv) was used as a characteristic (light) biocatalyst particle. These brown particles had an average diameter of 1.25 ± 0.004 mm and an average density of $1{,}100 \pm 6.6$ kg/m^3. We have used pelletized CaY zeolite particles as dense adsorbent particles. The manufacturing procedure was essentially equal to the procedure described by Vos et al. (1990). This resulted in 1.27 ± 0.05 mm, $1{,}362 \pm 2.6$ kg/m^3 white particles. Consistent with earlier work (Van der Wielen et al., 1997b), the light (dark) particle type is referred to as particle type II, and the dense (white) particle type as type III. The particles were fluidized in tap water at room temperature (298 K). Terminal velocities as well as Richardson and Zaki indexes (1955) of both particle species were estimated from expansion experiments. The terminal velocity of (light) particle type II was 0.0333 m/s and its Richardson and Zaki index was 3.29, whereas the terminal velocity of (dense) particle type III was 0.0729 m/s and its Richardson and Zaki index was 3.19.

For solids mixing experiments, the particles are colored with malachite green (type II particles, green–originally brown) and methylene blue (type III particles; blue—originally white). For solids mixing experiments, the contents of 1–3 pulsations were collected and the colored fraction of a 200-particle portion was determined.

Plate design

For pulsed-flow experiments, 5 Teflon plates were mounted at 0.15 m intervals at a central axis. The plates had a fixed, total free area of 10.6% that was distributed evenly over four conical holes, similar to the plate described by Vos et al. (1990). The angle of the cone was 45°, resulting in a 6.5-mm hole at the tapered side. Vos et al. (1990) indicated a critical ratio between hole and particle diameter of about 4–5, below which severe blockage of the holes occurred. Above this ratio, the volume of the transported particles was proportional to the pulse volume. See Figure 4, which is taken from the work of Vos et al., for the influence of the ratio of hole and particle diameter on the transported amount of solids. We have investigated the pulse-flow transport with type II and III particles (see earlier) with an average diameter of approximately 1.3 mm. Hence, the ratio of hole and particle diameter ($D/d = 5$) justifies the assumption of limited blockage. See the original work of Vos et al. (1990) for a more detailed description of the plate design.

Results

Visual observations

The densities and the diameters of particle types II and III were selected such that segregation always occurs, according to Eq. 6. For any combination of phases and liquid velocity, an upper zone of light particle (type II) always rested on a

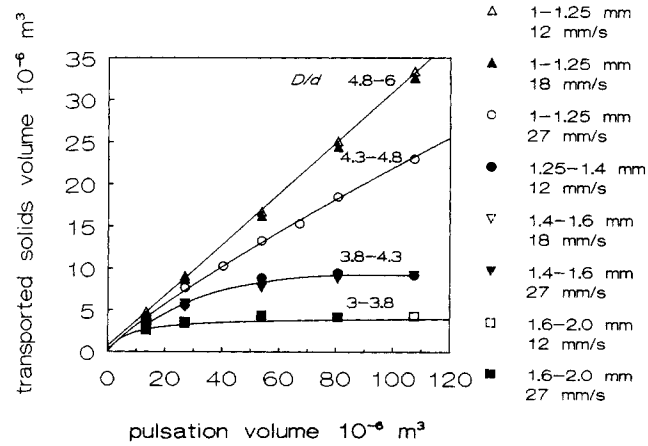

Figure 4. Influence of particle-hole diameter ratio in a multistage, water fluidized-bed contactor.

Particles: density 1320 kg/m^3; 6-mm hole; and 7.3% free area (after Vos et al. (1990)).

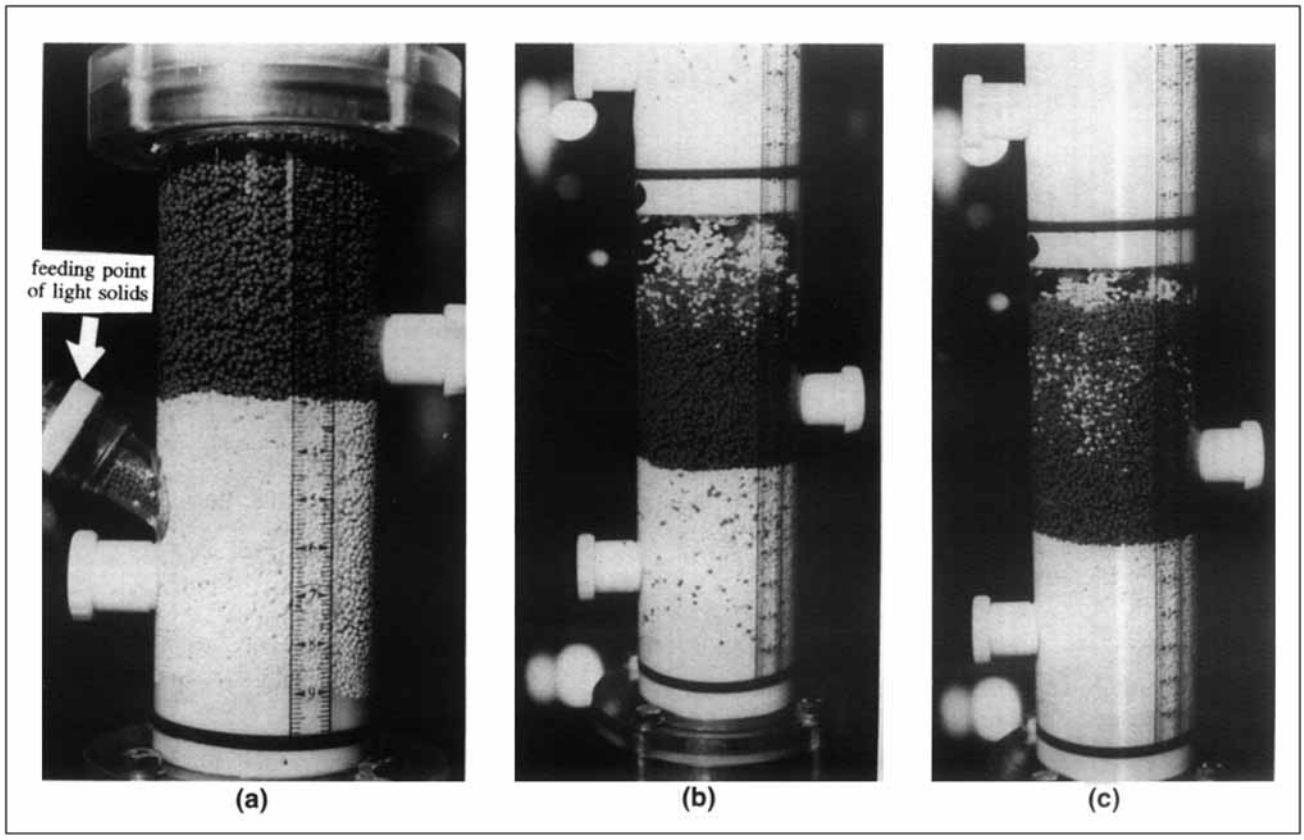

Figure 5. (a) Single stage of a multistage fluidized bed containing a segregated bed of dense (white) and light (dark) particles; (b) transport of dense (white) particles through a fluidized bed of light (dark) particles to a lower compartment; (c) transport and segregation of dense (white) and light (dark) particles; relative to Figure 5b, the fluidized bed is expanded due to the increased particle holdup as well as bulk density.

lower zone of dense adsorbent (type III). Figure 5a is a photograph of steady-state fluidization of the dense and light particles in the binary-solids multistage fluidized-bed reactor. The subsequent parts of the figure (5b and 5c) demonstrate the course of a complete pulsation cycle: 5b—transport of the (white) dense solids to a lower stage; 5c—segregation of the swarm of dense particles in a fluidized bed of the light (brown) particles. The subsequent stage is refluidization leading again to Figure 5a.

At relatively low pulsation frequencies ($f_p < 0.1$ Hz) and low pulsation volumes ($V_p \leq 15\ \mu m^3$), the cycle time is sufficient for complete segregation of the light and dense phases, and for subsequent relaxation of the bed to its steady-state situation. At these conditions, the particle fraction of the back-pulsed volume is approximately 38%. At high pulsation frequencies and volumes, the fluidized-bed dynamics of subsequent pulsations interfere. This resulted in vigorous turbulent phenomena as well as low and drastically varying solids fractions, especially at large pulsation volumes. In this case, the bed dynamics, in the form of shock waves, determines the minimum cycle time. We have tried to moderate the bed behavior by extending the actual pulsation time by a slower float movement, but this approach was not successful. At increased pulsation frequencies with smaller volumes, less interference was observed. The maximum frequency was mainly determined by the settling time of the dense particles (through the bed of light particles).

It should be noted that the fluidized bed of the light particles expands when the dense particles segregate. This can be illustrated by comparing bed levels in Figures 5b and 5c, which have been taken in a fluidized bed with a constant number of light (dark) particles. The expansion is attributed partially to the increased total amount of the fluidized particles, but also the increase in bulk density in the "mixture" of dense and light particles, which was also observed elsewhere (Wielen et al., 1997b). In case of large density differences, this may lead to unwanted washout of light particles to the upper compartment.

Pulsed-flow operation: solids and liquid fluxes

Solids Transport. Figure 6 illustrates the dependence of the solids transport on the back-pulsed flow for type III particles. The superficial liquid velocity was 1.2 cm/s ($\phi_L = 15 \times 10^{-6}$ m^3/s). The solid curve is calculated using Eq. 7 for a liquid fraction ϵ_L of 0.87. Distinct deviations from this relation occur at larger pulsation volumes. This is indicated by the filled squares connected by the dotted curve. This deviation implies a decline in the solids fraction of the pulsations, probably due to blockage of the holes. Additional results of the solids flow as a function of the back-pulsed flow for various pulsation frequencies are shown in Figure 7. The superficial liquid velocity was 1.2 cm/s as well. At higher pulsation frequencies (and low pulsation volumes), the solids holdup

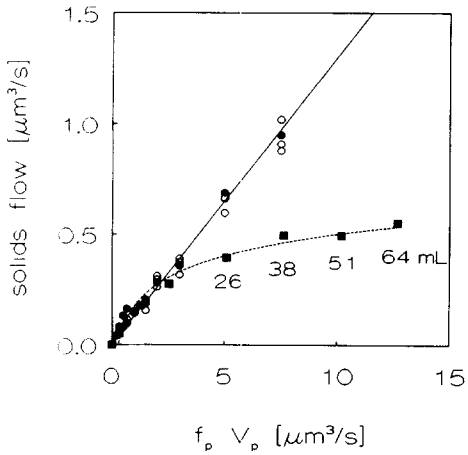

Figure 6. Type III solids transport vs. pulsed backflow.

○, $V_p \leq 15$ mL; ●, idem, binary in ii; ■, $V_p > 15$ mL (actual volumes given); ——, Eq. 7; ..., (dotted curve) behavior at high solids flow.

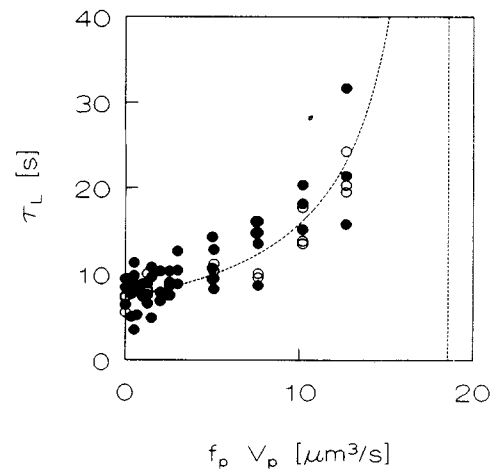

Figure 8. Liquid residence time as a function of the pulsed backflow.

Closed (type III); open type (II and III); .... (dotted curve) Eq. 10 with $C = 0.54$.

approaches the "ideal" situation of small volumes and low frequencies, which is described by Eq. 7 (solid curve). The dotted curves in Figure 7, which are drawn by inspection for various pulsation frequencies (0.1, 0.2 and 0.5 Hz), show the observed tendency of the deviation from Eq. 7 with increasing pulsation volume.

Furthermore, Figure 7 demonstrates an increased scattering of the data at low pulsation frequencies and large pulsation volumes. This is most likely due to blockage of the holes by the random stacking of particles. At higher frequencies, the higher turbulence of the liquid flow favors a smoother particle flow and less particle stacking. It is expected that a further enlargement of the holes enhances the particle transport and reduces the blocking of the hole.

Liquid Transport. Figure 8 shows the liquid residence time τ_L, determined from residence-time distribution measurements, as a function of the back-pulsed flow $f_p \cdot V_p$. The superficial liquid velocity was 1.2 cm/s during the steady-state fluidization period. These data concern monocomponent fluidized beds of type III particles as well as binary fluidized beds of type II and III particles. The vertical dotted line indicates the maximum back-pulsed flow, which is determined by an overall zero liquid flow. At this condition, no liquid can be fed to the column and the column contents are continuously pulsed up and down. As anticipated in an earlier section in this work, the liquid residence time correlates well with the back-pulsed flow. The liquid residence time increases drastically when the back-pulsed flow increases. The dotted curve is a best fit of Eq. 10 to the data. This corresponds with a value of $C = 0.54$ in Eq. 10. This value is significantly smaller than the liquid fraction in the back-pulsed volume, which was approximately 0.86. This is partially due to the way the liquid feed is switched on and off, which was gradual. Especially during the refluidization, the liquid flow was increased in an exponential manner to its setpoint to reduce the "overshoot" phenomena indicated in our previous work (Van der Wielen et al., 1997a).

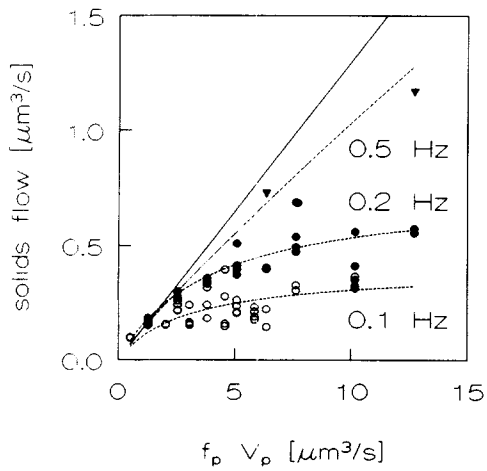

Figure 7. Solids transport as a function of the pulsed backflow for type III particles.

○, 0.1 Hz; ●, 0.2 Hz; ▼ 0.5 Hz; ——, Eq. 7; ..., (dotted curve) behavior at high solids flow.

Liquid and solids mixing

Liquid Mixing. Residence-time distribution measurements have been recorded for pulsation frequencies in the range of 0–0.5 Hz and for pulsation volumes of $0–64 \cdot 10^{-6}$ m^3 in four compartments of the laboratory scale MFB-contactor. The superficial liquid velocity was 1.2 cm/s for all experiments. The signals have been normalized to obtain E-curves. Of course, these signals clearly demonstrate the effect of the pulsations. A characteristic set of pulse-response measurements from compartments 3 and 4, respectively, at a high pulsation frequency ($f_p = 0.2$ Hz and $V_p = 63.6 \cdot 10^{-6}$ m^3) is shown in Figure 9. The jagged shape of the peaks is due to pulsations superimposed on the mean residence-time distribution curve of both input and output signals. The smooth, thick line is the model prediction of the axial dispersion model for the output signal, calculated by the inverse Fast Fourier Transform of the Fourier-domain convolution of input signal and the transfer function of the fluidized bed. The superimposed "pulsation" peaks have disappeared from the calcu-

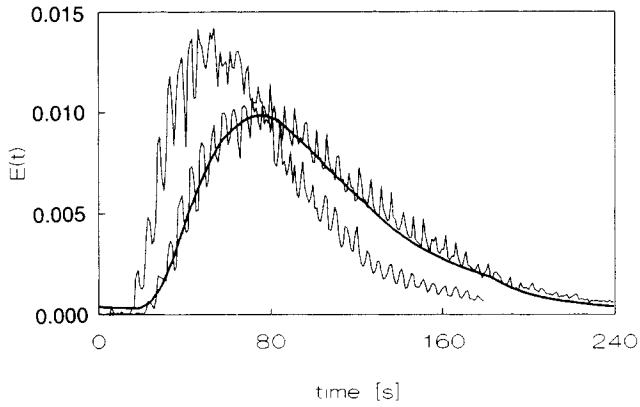

Figure 9. Pulse-response measurement and calculated response (thick curve) from the axial dispersion model.

$\tau_L = 31.69$ s, $Pe = 1.14$; other conditions indicated in text.

lated output signal due to the smoothing effect of the axial dispersion model.

The extent of mixing of the liquid phase was determined by fitting the experimental residence-time distribution curves measured in two succeeding compartments using the procedure outlined before, which led to the *Pe* numbers shown in Figure 10. The degree of plug flow of the liquid phase in the absence of the pulsations was expected to be high. This is confirmed by the experimental results shown in Figure 10 for monocomponent (type III particles) and binary beds (type II and III particles). Again the superficial velocity was 1.2 cm/s and the vertical dotted line indicates the maximum back-pulsed flow. Figure 10 shows the *Pe* number as an exponentially declining function of the back-pulsed flow $f_p \cdot V_p$. The *Pe* number decreased to a value of about 2–4, which corresponds to the situation of near-to-complete mixing. The reasons are partially the increased turbulence due to pulsation, and partially to the drastic increase in the liquid residence time at high $f_p \cdot V_p$. The data are scattered, as is usual for axial dispersion measurements (Chung and Wen, 1968; Krishnaswamy et al., 1978). For dispersion measurements with pulsations, this is likely to be even worse. The axial dispersion model is only an indication of the extent of liquid mixing and is not a mechanistic description of the actual liquid behavior.

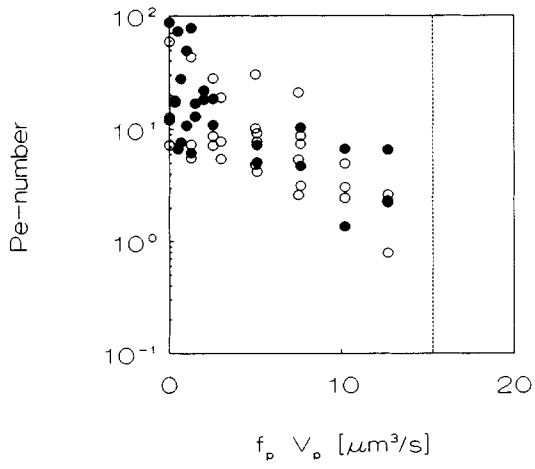

Figure 10. Liquid mixing as a function of the pulsed backflow.

Particles type III: closed (type III); open (binary bed of type II and II).

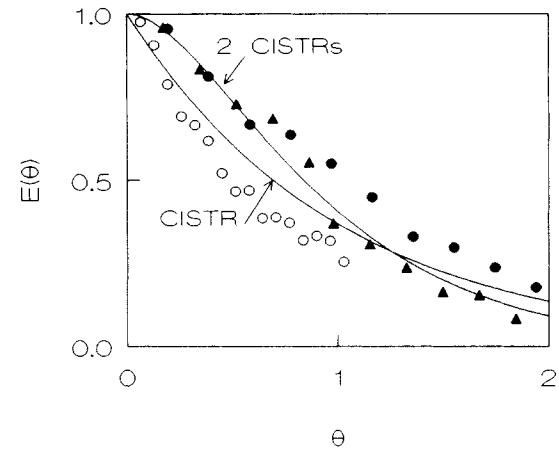

Figure 11. Solids mixing for various pulsation frequencies for type III particles.

●, 0.5 min^{-1}; ▲, 1.0 min^{-1}, ○, 1.3 min^{-1}; curves, model predictions for 1 and 2 CISTRs in series.

Solids Mixing. Particle collection in our experimental setup was only possible at moderate solids flows. Too high solids flows resulted in problems with solids withdrawal from the bottom of the column (changing and replacing flasks), and the necessarily short time interval between two samples. Hence, samples have only been collected for pulsation frequencies of 0.5, 1.0, and 1.3 min^{-1} and for a pulsation volume of 25μm^3. The experimental residence-time distribution curves for step-response experiments of the tracer particles of type II are shown in Figure 11 for these pulsation frequencies. The dimensionless time is computed from the experimentally determined overall solids flow rate (colored and noncolored particles). The predictions of the step response of one and two tanks in series are also drawn in this figure. It can be seen that the extent of mixing in each of these experiments is close to complete mixing. There is a slight tendency for improved mixing at increasing pulsation frequencies.

Discussion

Stable segregation

The criterion function F (Eq. 6) was used to predict whether or not stable segregation can occur for a given binary particle system and operating conditions. For the combination of light and dense particles in this work, the criterion function predicts complete segregation over the whole range of liquid velocities and overall bed compositions. This is in agreement with the experimental observations. The model has also been verified for other combinations (not presented here), and describes well motion and equilibrium in binary particle systems.

Is the countercurrent flow sufficiently large?

One of the most urgent questions before applying a pulsed multistage fluidized-bed contactor as a countercurrent ad-

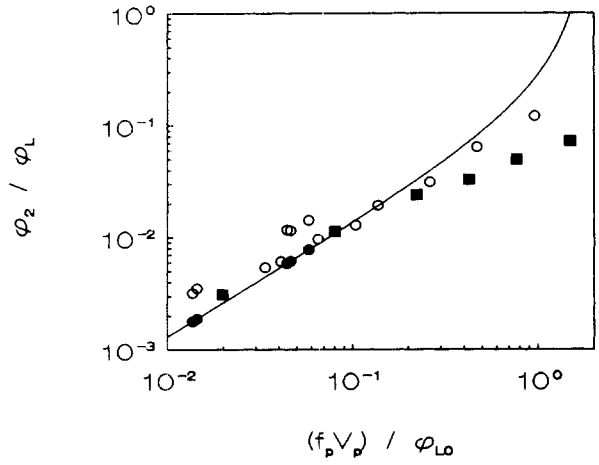

Figure 12. Solids and liquid flow ratio in pulsed flow.

○, $V_p \leq 15$ mL; ●, idem, binary in II; ■, $V_p > 15$ mL; calculated from Eq. 12.

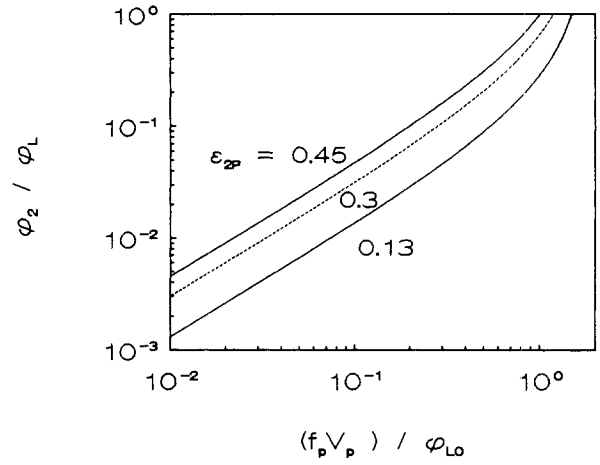

Figure 13. Simulated ratios of solids and liquid flow using Eq. 12 for various solids fractions in the pulsation volume.

$\epsilon_{2p} = 0.13$, 0.3, and 0.45; conditions as in Figure 12.

sorptive reactor is whether or not the solids flow is sufficiently large. Of course, this question can only be answered quantitatively when more details about the actual reaction–adsorption system are known (Van der Wielen et al., 1995, 1996b). Most essential is the magnitude of the reactant feed, and thus the maximum product flow in relation to the maximum capacity of the adsorbent flow to actually adsorb all product. For most practical systems, it can be estimated that the adsorbent flow should be at least 10% of the liquid flow on a volume basis (Van der Wielen et al., 1995, 1996b). In Figure 12, we have plotted the experimentally observed ratios of the flows of dense solids (type III particles) and liquid as a function of the back-pulsed flow $f_p \cdot V_p$. This quantity appears to be the key operational parameter in controlling the performance of the system. In previous sections, models were presented as a function of $f_p \cdot V_p$ for the net liquid and solids flows. Then the ratio of solids and liquid flow rates can be predicted as well. The corresponding expression reads:

$$\frac{\phi_2}{\phi_L} = \frac{\epsilon_{2p}\dfrac{\phi_p}{\phi_{Lo}}}{1 - C\dfrac{\phi_p}{\phi_{Lo}}} \quad \text{and} \quad \phi_p = f_p V_p. \tag{14}$$

This relation is presented as the solid curve drawn in Figure 12 with $C = 0.54$ and $\epsilon_{2p} = 0.13$. The solids fraction of the pulsation volume is fairly low when compared to the data of the other authors listed in Table 1. The reasons for this are probably a limiting hole-to-particle diameter ratio, and the apparent "sticking" of the particles due to nonperfect sphericity. It is obvious that increasing the solids fraction of the pulsation volume at otherwise constant conditions, increases the ratio of solids and liquid flow proportionally. Simulations with the average solids fractions reported by Van der Meer (1984) ($\epsilon_{2p} = 0.45$) and Vos et al. (1990) ($\epsilon_{2p} = 0.3$) are plotted in Figure 13, together with the best fit of the experimental results ($\epsilon_{2p} = 0.13$). It is anticipated that a further increase in the hole diameter (one large hole instead of four smaller) will lead to an increase in the solids fractions, and thus to better performance.

Sufficient plug flow of the liquid and solids phases?

The performance of countercurrent mass-transfer processes usually benefits from a high degree of plug-flow behavior in either phase. It is expected that a similar reasoning is true for countercurrent adsorptive reactors. In fact, dispersion in both phases should even be smaller than for nonreactive conditions, as mixing of reactant and unloaded adsorbent might lead to undesired reactant adsorption. Likewise, mixing of product and catalyst may lead to further unwanted or reverse reaction of the product. Both situations mean large equipment, a loss of reactant or product, and a decrease in overall yield.

Earlier sections have indicated an exponential increase in the extent of liquid mixing that is close to the predicted operating conditions of the reactor. The maximum of liquid mixing is complete liquid mixing at each stage. However, up to fairly high solids transport rates (and correspondingly high pulsation frequencies and volumes), the *Pe* number for the liquid mixing in one compartment was still around 10. The solids mixing at moderate pulsation frequencies is nearly complete at one stage of the multistage configuration. Therefore, the worst case—maximum mixing of the solids and liquid phases—corresponds to complete liquid and complete solids mixing at one stage. In other words, the minimum number of mixing units equals the number of stages. The total degree of plug-flow behavior of either phase can be improved by increasing the number of stages. However, without further details about the actual reaction–adsorption system, it is impossible to predict a sufficient minimum number of stages for the worst case of liquid and solids mixing.

Conclusion

Pulsed multistage fluidized-bed equipment has interesting possibilities for the selective counterflow of dense particles in fluidized beds of lighter particles. Key factors in the equipment performance are the ratio of dense solids-to-liquid flow and the extent of mixing in the solids and liquid phase. Rational selection of binary particle mixtures, equipment size,

and operating conditions on the basis of these key factors is necessary for reliable design.

In this article, a set of design tools for the selection of particle mixtures, ratio of solids-to-liquid flow, and the extent of mixing as a function of operating conditions (pulsation frequency and volume) has been presented as mathematical relations and evaluated for a relevant set of experimental conditions. The reasonable to good agreement of experimental results and design tools supports their use for the design of larger-scale pulsed-flow equipment.

Acknowledgments

The Netherlands Organization for Scientific Research (NWO) is gratefully acknowledged for its financial support, as is Gist-brocades NV for the free Maxazyme GI Immob. The Mechanical and Electronic Workshop of the Kluyver Laboratory for Biotechnology is thanked for the technical assistance during the construction of the laboratory-scale contactor.

Notation

A = area, m^2
c = dimensionless tracer concentration
Pe = Peclet number
u_L = linear liquid velocity, m/s
u_i = linear velocity of species i relative to the observer, m/s
v_{ij} = (linear) slip velocity of phases i and j, m/s
$v_{Li\infty}$ = terminal velocity of species i, m/s
z = dimensionless axial coordinate
ϕ = flow rate, m^3/s
ϕ_{Lo} = flow rate during steady-state fluidization, m^3/s
ρ = density, kg/m^3
θ = time relative to liquid residence time

Subscripts

i = phase i
o = superficial
1,2 = light and dense solids phases

Literature Cited

Bennett, B. A., F. L. D. Cloete, and M. Streat, "A Systematic Analysis of the Performance of a New Continuous Ion-Exchange Technique," *Ion Exchange Proc. Ind.*, 133 (1984).

Chung, S. F., and C. Y. Wen, "Longitudinal Dispersion of Liquid Flowing Through Fixed and Fluidized Beds," *AIChE J.*, **14**(6), 857 (1968).

Cloete, F. L. D., and M. Streat, Brit. Patent No. 1,070,251 (1962).

Cloete, F. L. D., and M. Streat, "A New Continuous Solid-Fluid Contacting Technique," *Nature*, **200**, 1199 (1963).

Dodds, R., P. I. Hudson, L. Kershenbaum, and M. Streat, "The Operation and Modeling of a Periodic, Countercurrent Solid-Liquid Reactor," *Chem. Eng. Sci.*, **28**, 1233 (1973).

DSM/Stamicarbon, U.S. Patent No. 4,209,591 (1980).

Fahim, M. A., and N. Wakao, "Parameter Estimation from Tracer Response Measurements," *Chem. Eng. J.*, **25**, 1 (1982).

Foscolo, P. U., and L. G. Gibilaro, "A Fully Predictive Criterion for the Transition Between Particulate and Aggregate Fluidization," *Chem. Eng. Sci.*, **39**(12), 1667 (1984).

Gibilaro, L. G., R. di Felice, S. P. Waldram, and P. U. Foscolo, "A Predictive Model for the Equilibrium Composition and Inversion of Binary Solid Liquid Fluidized Beds," *Chem. Eng. Sci.*, **41**(2), 379–387 (1986).

Groen, D. J., "Macromixing in Bioreactor," PhD Thesis, Delft Univ. of Technology, Delft, The Netherlands (1994).

Jean, R.-H., and L. S. Fan, "On the Criteria of Solids Layer Inversion in a Liquid-Solid Fluidized Bed Containing a Binary Mixture of Particles," *Chem. Eng. Sci.*, **41**(11), 2811 (1986).

Khang, S. J., and T. J. Fitzgerald, "A New Probe and Circuit for Measuring Electrolyte Conductivity," *Ind. Eng. Chem. Fundam.*, **14**(3), 208 (1975).

Krishnaswamy, P. R., R. Ganapathy, and L. W. Shemilt, "Correlating Parameters for Axial Dispersion in Liquid Fluidized Systems," *Can. J. Chem. Eng.*, **56**, 550 (1978).

Moritomi, H., T. Iwase, and T. Chiba, "A Comprehensive Interpretation of Solid Layer Inversion in Liquid Fluidized Beds," *Chem. Eng. Sci.*, **37**(12), 1751 (1982).

Moritomi, H., T. Yamagishi, and T. Chiba, "Prediction of Complete Mixing of Liquid Fluidized Binary Solid Particles," *Chem. Eng. Sci.*, **41**(2), 297 (1986).

Richardson, J. F., and W. N. Zaki, "Sedimentation and Fluidisation: I, *Trans. Inst. Chem. Engrs.*, **32**, 35 (1954).

Van der Meer, A. P., "On Countercurrent Fluidized Ion Exchange Columns," PhD Thesis, Delft Univ. of Technology, Delft, The Netherlands (1984).

Van der Wiel, J. P., and J. A. Wesselingh, "Continuous Adsorption in Biotechnology," A. E. Rodriques, M. D. LeVan and D. Tondeur, eds., *Adsorption: Science and Technology*, Kluwer, Amsterdam, p. 427 (1989).

Van der Wielen, L. A. M., J. J. M. Potters, A. J. J. Straathof, and K. Ch. A. M. Luyben, "Integration of Bioconversion and Continuous Product Separation by Means of Countercurrent Adsorption," *Chem. Eng. Sci.*, **45**(8), 2397 (1990).

Van der Wielen, L. A. M., P. J. Diepen, A. J. J. Straathof, and K. Ch. A. M. Luyben, "Two New Countercurrent Adsorptive Enzyme Reactors. Operational Conditions for Deacylation of Penicillin G," *Ann. N. Y. Acad. Sci.*, **750**, 482 (1995).

Van der Wielen, L. A. M., M. H. H. van Dam, and K. Ch. A. M. Luyben, "On the Relative Motion of a Sphere in a Swarm of Different Spheres," *Chem. Eng. Sci.*, **51**(6), 995 (1996a).

Van der Wielen, L. A. M., P. J. Diepen, J. Houwers, and K. Ch. A. M. Luyben, "A Countercurrent Adsorptive Reactor for Acidifying Bioconversions," *Chem. Eng. Sci.*, **51**(10), 2315 (1996b).

Van der Wielen, L. A. M., A. W. K. G. Sjauw-Koen-Fa, J. J. M. Potters, and K. Ch. A. M. Luyben, "Transient Behavior of Pulsed Particulate Fluidized Beds," *AIChE J.*, **43**(3), 625 (1997a).

Van der Wielen, L. A. M., M. H. H. van Dam, and K. Ch. A. M. Luyben, "Trickle Flow of Dense Particles Through a Fluidized Bed of Others," *Chem. Eng. Sci.*, **52**(4), 553 (1997b).

Van Duijn, G., and K. Rietema, "Segregation of Liquid-Fluidized Solids," *Chem. Eng. Sci.*, **37**(5), 727 (1982).

Vos, H. J., C. van Houwelingen, M. Zomerdijk, and K. Ch. A. M. Luyben, "Countercurrent Multistage Fluidized Bed Reactor for Immobilized Biocatalysts: III. Hydrodynamic Aspects," *Biotechnol. Bioeng.*, **36**, 387 (1990).

Manuscript received Feb. 7, 1997, and revision received Sept. 29, 1997.